A Simple Decoupling Network With Filtering Response for Patch Antenna Arrays

Zhang, Yiming; Ye, Qi-Cheng; Pedersen, Gert Frølund; Zhang, Shuai

Published in:
I E E E Transactions on Antennas and Propagation

DOI (link to publication from Publisher):
10.1109/TAP.2021.3070632

Publication date:
2021

Document Version
Accepted author manuscript, peer reviewed version

A Simple Decoupling Network With Filtering Response for Patch Antenna Arrays

Yi-Ming Zhang, *Member, IEEE*, Qi-Cheng Ye, *Student Member*, *IEEE*, Gert Frølund Pedersen, *Member, IEEE*, and Shuai Zhang, *Senior Member, IEEE*

***Abstract*—Facing the demand for decoupling and filtering for large-scale antenna arrays in modern communication systems, a transmission-line-based scheme is proposed and studied in this article. Different from other decoupling networks published recently featuring narrow decoupling bandwidths and high spurious levels, the proposed approach uses simple T-shaped networks where decoupling and filtering responses are realized simultaneously, leading to high frequency selectivity and improved decoupling bandwidth. The proposed design is a simple one-dimension configuration but powerful for two-dimension arrays. Based on the study case of a 4×4 dual-polarized patch array, theoretical analysis and full-wave simulation are carried out to verify the performance in the decoupling and frequency selectivity of this method. A prototype is further fabricated, assembled, and measured to demonstrate the performance of the proposed method in practice. The measured and simulated results are consistent with each other where a low insertion loss of around 0.6 dB is observed. The results denote that the proposed method is easily realized with a very small effect on the radiation performance of antenna elements, making it to be a potential and valuable decoupling and filtering solution for large-scale arrays.**

***Index Terms*—Active impedance matching, decoupling, filtering, massive multiple-input and multiple-output.**

I. Introduction

As an important task for large-scale array systems, for instance, massive multiple-input multiple-output (MIMO) and phased arrays, mutual coupling suppression becomes an active research area and attracts increasing attention recently [1]-[5]. In terms of communication capacity, beam scanning ability, and linearity of power amplifiers, the influence of the mutual coupling among antenna elements on the performance of systems can be negligible if the coupling is suppressed to a low level. A 17-dB isolation level among antenna elements is normally sufficient for MIMO transmission from the error rate and envelope correlation coefficient point of view [5]. However, for large-scale antenna array systems, an isolation level of 17 dB is not high enough since additional considerations are involved under beam scanning conditions. First of all, the active impedance of the antenna elements would be significantly influenced when doing beam steering if the mutual coupling is not suppressed to a very low level [6]-[9]. It has been verified in [6] that with 15-dB isolation, the maximum VSWR of the elements in a linear array is almost six, which is still higher than two even the isolation is enhanced to 20 dB. In [8] and [9], it is found that the active VSWR of the MIMO antennas is almost less than two once the mutual coupling can be suppressed to less than −25 dB. Besides, active impedance mismatching would significantly change the load impedance values of the power amplifiers, which would further lead to nonlinear distortion and may decrease the amplifier efficiency. Thus, an isolation level of 25 dB is normally required for a massive MIMO antenna array. In the past decade, many efforts have been devoted to dealing with the coupling issue, such as electromagnetic bandgap structure [10], *LC*-based network [11], distributed-circuit-based scheme [12]-[14], decoupling metasurface [15], defected ground [16] and scatter-loaded scheme [17]. Most of these approaches were proposed for two- or three-element arrays, at the cost of large element distances, high insertion losses, bulky system sizes or the isolation level is not high enough for massive MIMO antenna arrays.

For large-scale arrays, some decoupling methods were reported more recently [7]-[9], [18]-[23]. In [7], a coupled-line-based decoupling network was studied for an E-coupled linear antenna array. For dual-polarized *M*×*N* patch arrays, a lattice-shaped decoupling network was given in [8]. Because of the strong resonance characteristic, the decoupling bandwidths were narrow. In [9], antenna decoupling surfaces were designed to suppress the mutual coupling of dual-polarized antenna arrays, at the cost of high profile since the surfaces were positioned approximately half-wavelength away from the antenna aperture. To further suppress the coupling between diagonal pair of elements, a phase compensation method for antenna decoupling surface was provided in [20], but only effective for the arrays with staggered distributions. Near field resonators and wavetrap structures were studied for large-scale arrays in [22] and [23], respectively. Due to the specified decoupling structure or limited physical dimensions, the two schemes are not effective for dual-polarized arrays.

According to the aforementioned reports, it is found that network-based decoupling methods are generally effective for dual-polarized arrays with low profiles and a very small effect

This work was supported by AAU Young Talent Program and Huawei project of "5G mmWave Decoupling Array". (*Corresponding author*: *Shuai Zhang*.)

The authors are with the Antenna, Propagation and Millimeter-wave Systems (APMS) Section, Aalborg University, Aalborg 9220, Denmark (e-mail: yiming@es.aau.dk, qcy@es.aau.dk, gfp@es.aau.dk, sz@es.aau.dk).

Qi-Cheng Ye is also with the School of Physics, University of Electronic Science and Technology of China, Chengdu 610054, China.

on radiation performance since there is no additional structure positioned in or around radiating structures. However, the decoupling bandwidth is restrained by the strong resonance characteristics of transmission lines. Besides, the out-of-band spurious level might raise [8], which would increase the burden of the subsequent filtering module from the entire system point of view.

On the other hand, antennas designed with filtering responses, called filtering antennas, have been a focused research area [24]-[30], since filters are also the essential components in modern communication systems. Here, high frequency selectivity, out-of-band spurious rejection, and system miniaturization can benefit from the integration design of antennas and filters. In general, there are two approaches to realize filtering antennas. The first one focuses on the investigation of radiating structure with filtering responses [24]-[26], and the second aims at the integration of antennas and filtering feedings [27]-[30]. For the former, a bulky dimension of the antenna itself is generally required since additional structures are essential. This is not suitable for large-scale arrays where a small element distance is needed. At this point, the latter would be a potential candidate for large-scale array applications to achieve filtering responses. Based on the above discussions, cascading a filter at the input interface of every decoupled antenna might be a solution to improve the frequency selectivity of antenna arrays, leading to a suppressed spurious. However, this kind of simple connection would result in large system sizes. Moreover, additional insertion losses were caused by the filter itself, and the filtering performance might be degraded due to the non-ideal matching at the connection between the filter and antenna [27].

In this paper, a simple T-shaped 1-dimension decoupling network with filtering responses is proposed and studied for 2-dimension large-scale patch antenna arrays. Please note that decoupling schemes using T-shaped bridges have been studied widely [12], [13], [19]. In [12], a T-shaped bridge was studied to generate two decoupling resonances for dual-band two-element arrays. In [13], a two-order decoupling network for dual-band two-element arrays was studied, where a T-shaped bridge was utilized for the decoupling of the lower operating frequency and keeping the independence between the decoupling stages of the two frequencies. In [19], a T-shaped network was utilized for decoupling and impedance matching improvement. Different from these works, the proposed scheme is not a simple cascade configuration but realizes the decoupling and filtering performance simultaneously by using a single T-shaped network. To the best of the authors' knowledge, this is the first report that both decoupling and filtering functions can be generated by using a simple network configuration. The main novelties and merits are as follows.

(1) The filtering network shares the same network for decoupling, leading to low insertion loss and compact size, where only a single PCB layer is required. The method can be widely utilized for large-scale dual-polarized antenna arrays.

(2) The transmission zeros for filtering at both the lower and upper frequencies can be generated and tuned independently with high frequency selectivity.

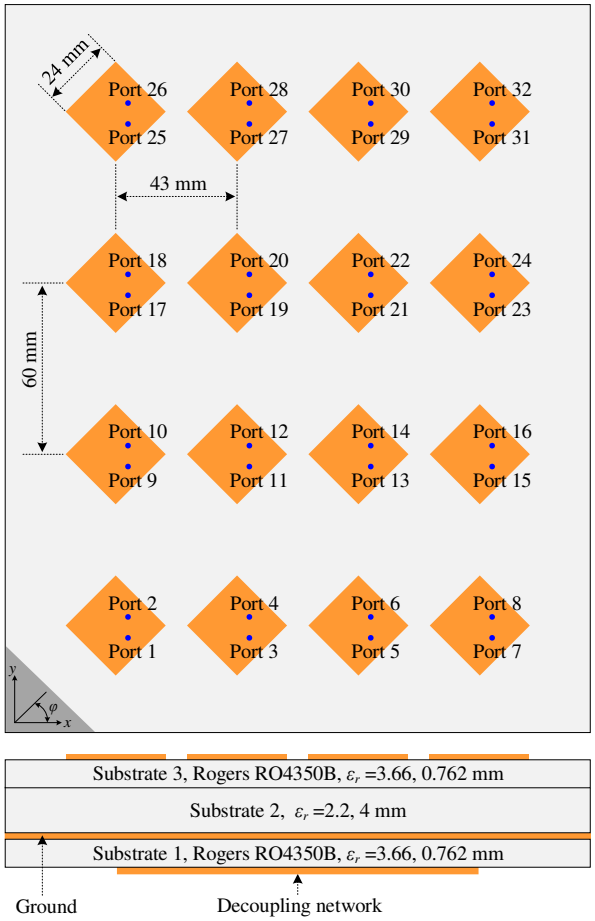

Fig. 1. Configurations of a 4×4 dual-polarized patch antenna array integrated with the proposed decoupling networks.

(3) Owing to the filtering property, the decoupling bandwidth is wider than the ones using other network-based methods, e.g., in [8]. The vertical and diagonal pairs of elements in large arrays are also decoupled, despite there is no direct decoupling structure for these elements.

This paper is organized as follows. Section II provides the theoretical analysis of the proposed network, including the decoupling, filtering as well as impedance matching. In Section III, graphical studies are further carried out to show the tuning of the filtering responses and the decoupling levels between the elements which are mentioned and not mentioned in Section II. Full-wave simulations and measurements of a demonstrator are summarized in Section IV. Array performance under scanning conditions is also provided. Finally, a conclusion is stated in Section V.

II. Analysis of the Proposed Decoupling Method

In this section, theoretical synthesis is operated to show the principles of decoupling and filtering. For ease of analysis, a 4×4 dual-polarized patch antenna array centered at 3.5 GHz is utilized as a study case, as shown in Fig. 1. The element distances in vertical and horizontal directions are different, representing $0.5\lambda_0$ and $0.7\ \lambda_0$ (λ_0 is the free space wavelength at the center frequency), respectively. In this article, the proposed networks operate directly on the horizontally allocated adjacent

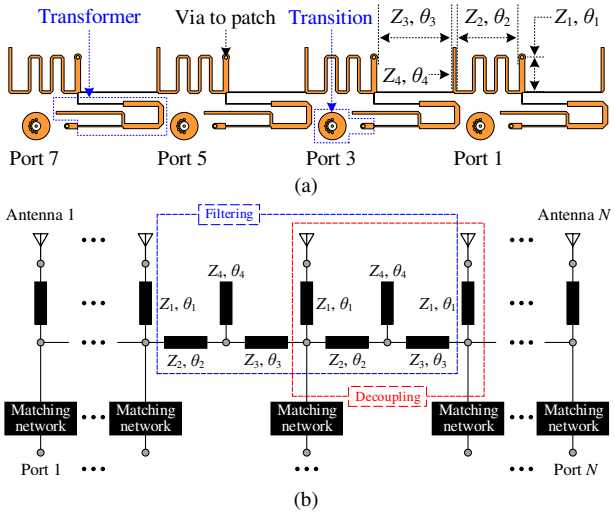

Fig. 2. Configurations of the proposed decoupling networks for the array given in Fig. 1. (a) Bottom view of the decoupling network for ports 1, 3, 5, and 7. (b) Equivalent circuit model of the decoupling network.

antennas with co-polarization. Seeing that the isolation between cross-polarized port is already high enough, there is no additional decoupling operation for the cross-polarized ports. The isolation between non-adjacent ports is normally high enough in patch antenna arrays, there is also no additional decoupling operation for these ports. This is a common consideration during the decoupling of large-scale arrays [7]-[9], [21]-[23]. Therefore, the basic decoupling principle is that the isolation between non-adjacent elements should not be degraded. Moreover, owing to the filtering response introducing by the decoupling networks for horizontal pairs, the mutual coupling levels between vertical and diagonal pairs of elements are also decreased. There is also no direct decoupling for these pairs, which will be discussed in the next section. Therefore, this work presents a 1-dimension method to decouple 2-dimension antenna arrays, featuring a very simple design procedure, filtering response, and compact size.

The physical layout of the proposed decoupling network with filtering responses is illustrated in Fig. 2(a), where ports 1, 3, 5, and 7 are selected as the representative ports. The realized network includes three parts, decoupling and filtering part, impedance matching part (Transformer part in Fig. 2(a)) as well as transition part for soldering MMCX connectors. Fig. 2(b) plots the equivalent circuit of the proposed network given in Fig. 2(a). It is depicted that the network is composed of T-shaped distributed circuits, where all the electrical lengths are referred to the center frequency f_0.

Next, the investigation of the proposed scheme will be operated in three parts. The principles of decoupling and filtering will be investigated in Part A. The realization of impedance matching and the design of transition for implementation will be discussed in Part B. A complete design procedure for dual-polarized arrays will be given in Part C.

A. Network analysis of the proposed structure

As illustrated in Fig. 2(b), the proposed network features both decoupling and filtering responses. For decoupling

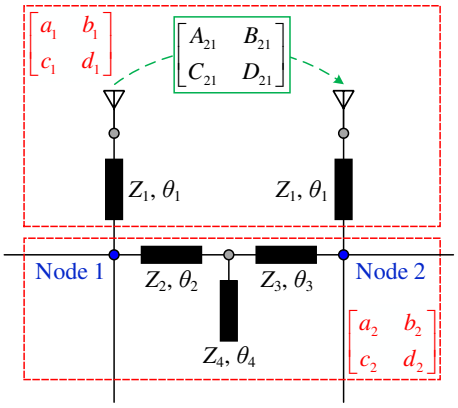

Fig. 3. Simplified equivalent circuit of the proposed scheme for decoupling investigation.

purposes, a simplified circuit is constructed, as shown in Fig. 3. The investigation of the T-shaped network given in [13] based on microwave network theory [31] is introduced for decoupling analysis, expressed as (1)-(8) in this article. More detailed, the transmission matrix between Nodes 1 and 2 through the antenna coupling is formulated as

$$\begin{bmatrix} a_1 & b_1 \\ c_1 & d_1 \end{bmatrix} = \begin{bmatrix} \cos\theta_1 & jZ_1\sin\theta_1 \\ j\dfrac{\sin\theta_1}{Z_1} & \cos\theta_1 \end{bmatrix} \begin{bmatrix} A_{21} & B_{21} \\ C_{21} & D_{21} \end{bmatrix} \times \begin{bmatrix} \cos\theta_1 & jZ_1\sin\theta_1 \\ j\dfrac{\sin\theta_1}{Z_1} & \cos\theta_1 \end{bmatrix} \tag{1}$$

where

$$\begin{aligned} b_1 = {} & (A_{21}\cos\theta_1 + jZ_1C_{21}\sin\theta_1)\,jZ_1\sin\theta_1 \\ & + (B_{21}\cos\theta_1 + jZ_1D_{21}\sin\theta_1)\cos\theta_1 \end{aligned} \tag{2}$$

On the other hand, the transmission matrix between Nodes 1 and 2 through the T-shaped bridge can be expressed as

$$\begin{bmatrix} a_2 & b_2 \\ c_2 & d_2 \end{bmatrix} = \begin{bmatrix} \cos\theta_2 & jZ_2\sin\theta_2 \\ j\dfrac{\sin\theta_2}{Z_2} & \cos\theta_2 \end{bmatrix} \begin{bmatrix} 1 & 0 \\ j\dfrac{\tan\theta_4}{Z_4} & 1 \end{bmatrix} \times \begin{bmatrix} \cos\theta_3 & jZ_3\sin\theta_3 \\ j\dfrac{\sin\theta_3}{Z_3} & \cos\theta_3 \end{bmatrix} \tag{3}$$

where

$$b_2 = (\cos\theta_2 - \frac{Z_2\sin\theta_2\tan\theta_4}{Z_4})\,jZ_3\sin\theta_3 + jZ_2\sin\theta_2\cos\theta_3 \tag{4}$$

For decoupling purposes, we have that

$$Y_{21}\Big|_{f=f_0} = -\frac{1}{b_1} - \frac{1}{b_2} = 0 \tag{5}$$

Then the following relations can be derived that

$$\left(\mathrm{Re}[C_{21}]Z_1^2\tan^2\theta_1 + \mathrm{Im}[A_{21}+D_{21}]Z_1\tan\theta_1 - \mathrm{Re}[B_{21}]\right)\Big|_{f=f_0} = 0 \tag{6a}$$

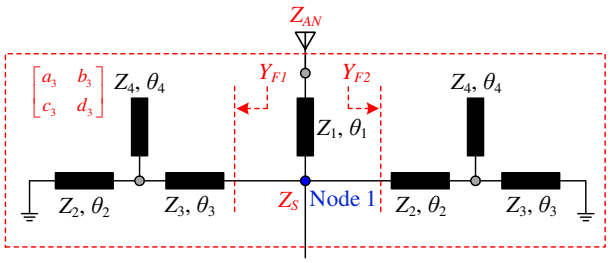

Fig. 4. Simplified equivalent circuit of the proposed scheme for filtering analysis.

$$\left.\frac{\tan\theta_4}{Z_4}\right|_{f=f_0} = \left.\frac{P_D + Z_2\sin\theta_2\cos\theta_3 + Z_3\cos\theta_2\sin\theta_3}{Z_2 Z_3 \sin\theta_2\sin\theta_3}\right|_{f=f_0} \quad (6b)$$

where

$$\begin{aligned} P_D = {} & \mathrm{Re}[A_{21}]Z_1\sin\theta_1\cos\theta_1 + \mathrm{Im}[B_{21}]\cos^2\theta_1 \\ & - \mathrm{Im}[C_{21}]Z_1^2\sin^2\theta_1 + \mathrm{Re}[D_{21}]Z_1\sin\theta_1\cos\theta_1 \end{aligned} \quad (7)$$

From (6a), it is derived that

$$\theta_1 = \arctan\left(\frac{-\mathrm{Im}[A_{21}+D_{21}] \pm \sqrt{\Delta}}{2\,\mathrm{Re}[C_{21}]Z_1}\right) \quad (8a)$$

$$\Delta = \mathrm{Im}^2[A_{21}+D_{21}] + 4\,\mathrm{Re}[B_{21}]\mathrm{Re}[C_{21}] \quad (8b)$$

It is found from (8) that for an arbitrarily given value of Z_1, there always has a solution for θ_1. Subsequently, a group solution of Z_4 and θ_4 can be further determined based on (6b) with given values of Z_2, Z_3, θ_2, and θ_3. The above analysis denotes that the decoupling between Nodes 1 and 2 can be achieved by following the derived descriptions shown in (6)-(8), where the parameters of Z_2, Z_3, θ_1, θ_2, and θ_3 are selected in advance.

Now consider the proposed network as working in filtering mode. Here, network analysis for filtering purposes is carried out, where a simplified circuit is further developed, as sketched in Fig. 4. It is seen that for the selected antenna element, two T-shaped networks are shunted at Node 1. Since the leaking power through the decoupling network is of a small part, compared to the total input power, the ends of the two T-shaped networks are open-circuited for simplification purposes. Then the transmission matrix between Node 1 and the input interface of the antenna element can be given by

$$\begin{bmatrix} a_3 & b_3 \\ c_3 & d_3 \end{bmatrix} = \begin{bmatrix} 1 & 0 \\ Y_{F1}+Y_{F2} & 1 \end{bmatrix} \begin{bmatrix} \cos\theta_1 & jZ_1\sin\theta_1 \\ j\dfrac{\sin\theta_1}{Z_1} & \cos\theta_1 \end{bmatrix} \quad (9)$$

where the input admittances seen looking into the T-shape networks are

$$Y_{F1} = j\frac{Z_3Z_4 - Z_2\tan\theta_2\left(Z_3\tan\theta_4 + Z_4\tan\theta_3\right)}{Z_3^2\tan\theta_3\left(Z_2\tan\theta_2\tan\theta_4 - Z_4\right) - Z_2Z_3Z_4\tan\theta_2} \quad (10a)$$

$$Y_{F2} = j\frac{Z_2Z_4 - Z_3\tan\theta_3\left(Z_2\tan\theta_4 + Z_4\tan\theta_2\right)}{Z_2^2\tan\theta_2\left(Z_3\tan\theta_3\tan\theta_4 - Z_4\right) - Z_2Z_3Z_4\tan\theta_3} \quad (10b)$$

On the other hand, the study in [32] provides the conversion

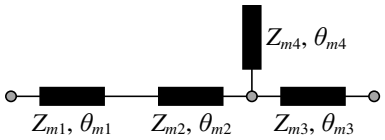

Fig. 5. Equivalent circuit of the chamfer mentioned in Fig. 1(b) for impedance matching.

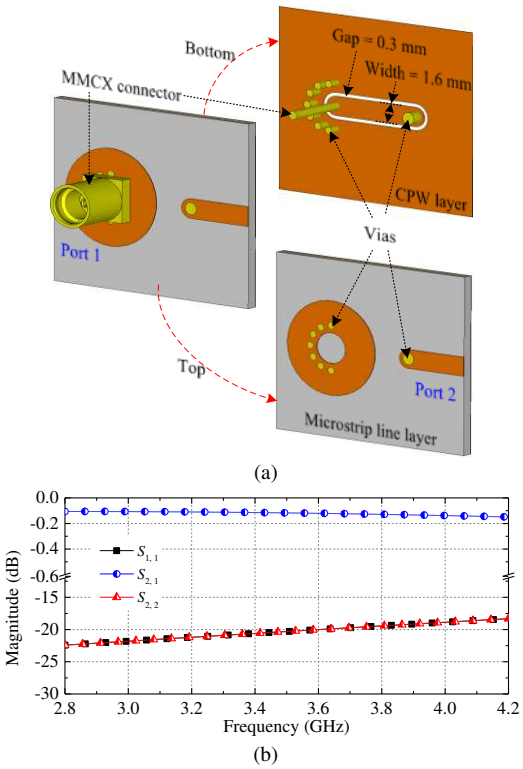

Fig. 6. (a) Configuration of the MMCX-to-CPW-to-microstrip line transition for testing purposes. (b) Full-wave simulated results of the transition.

relationships between S parameters and transmission parameters of a two-port network, expressed as

$$S_{L,S} = \frac{2\sqrt{R_S R_L}}{a_0 Z_L + b_0 + c_0 Z_S Z_L + d_0 Z_S} \quad (11)$$

where the parameters Z_S and Z_L are the source and load impedances, respectively, and the parameters R_S and R_L are the real parts of the source and load impedances correspondingly. The parameters a_0, b_0, c_0, and d_0 represent the transmission parameters of the network. As for the circuit model plotted in Fig. 4, the load impedance Z_L is equal to the input impedance of the antenna Z_{AN}, and Node 1 is considered as the source. Facing the filtering purposes, it is assumed that transmission zeros are generated at the selected frequencies f_1 and f_2, where $f_1 < f_0 < f_2$. Substituting (9) and (10) into (11), it is found that the transmission coefficient $S_{L,S}$ would be zero at the frequencies of f_1 and f_2 under the following relations

$$\left[Z_3\tan\theta_3\left(Z_2\tan\theta_2\tan\theta_4 - Z_4\right) - Z_2Z_4\tan\theta_2\right]_{f=f_1} = 0 \quad (12a)$$

$$\left[Z_2\tan\theta_2\left(Z_3\tan\theta_3\tan\theta_4 - Z_4\right) - Z_3Z_4\tan\theta_3\right]_{f=f_2} = 0 \quad (12b)$$

From the derived relations of (12), transmission zeros would be obtained at the frequencies f_1 and f_2, resulting in bandpass responses.

Based on the aforementioned discussions, a decoupling network with filtering responses can be fully determined from the relations of (6)-(8) and (12). The next part will discuss the matching network and the transition for implementation purposes.

B. Impedance matching and implementation for testing

Seeing that the impedance matching is not involved during the numerical studies in Section II, a T-shaped multi-section transformer is utilized to compensate for the mismatching caused by the decoupling and filtering, as mentioned in Fig. 2(a) and shown in Fig. 5. Once the decoupling network is determined, the parameter values of the matching network can be readily derived by using the network synthesis method [31], which is not detailed for brevity. Although additional insertion losses would be introduced by the four-order transformer, the total efficiency of the array using the proposed scheme is still kept at a high level. This will be discussed and verified in Section IV, where a prototype is manufactured and measured.

For implementation and testing purposes, MMCX connectors are employed and a microstrip-to-CPW transition is presented, as mentioned in Fig. 2(a) and illustrated in Fig. 6(a). The end of the microstrip line connects to the input node of the decoupling network, and the end of the CPW line is fed by the MMCX connector directly. To further show the transmission performance of the transition, full-wave simulations are carried out. The results are plotted in Fig. 6(b). It is observed that the transition is well-matched with a very low insertion loss of approximately 0.15 dB within the studied frequency band. After integrating the impedance matching networks and the transitions for testing in practice, a network that features decoupling and filtering is developed.

C. Design procedure of the proposed scheme

To describe the realization of the proposed scheme more clearly, a design flowchart is given as shown in Fig. 7, and a design procedure is further summarized as follows.

Step 1: Conforming the specifications, such as substrate parameters, center frequency f_0, transmission zeros at the desired frequencies f_1 and f_2, and extracting the mutual coupling matrix among antennas through full-wave simulations.

Step 2: Determining the values of Z_1, Z_4, and θ_4 with given values of Z_2, Z_3, θ_2, and θ_3 by using (6)-(8). As mentioned, the parameters of Z_2, Z_3, θ_1, θ_2, and θ_3 are selected in advance. This step aims to find the relations of the parameters under decoupling mode.

Step 3: Evaluating and checking whether the determined values obtained from *Step 2* satisfy the condition (12). If not, a new group of Z_2, Z_3, θ_1, θ_2, and θ_3 would be selected, and the others need to be renewed through *Step 1* until they fit (12). This step gives further requirements for the parameters under filtering mode. Please note that in this step, dozens or hundreds of iterations are normally required. Choosing a proper optimization algorithm can achieve the purposes readily and quickly. In this article, the random optimization method provided by the Advance Design System, an electronic design automation software, is utilized to establish the lossless transmission-line mode and determine the parameter values.

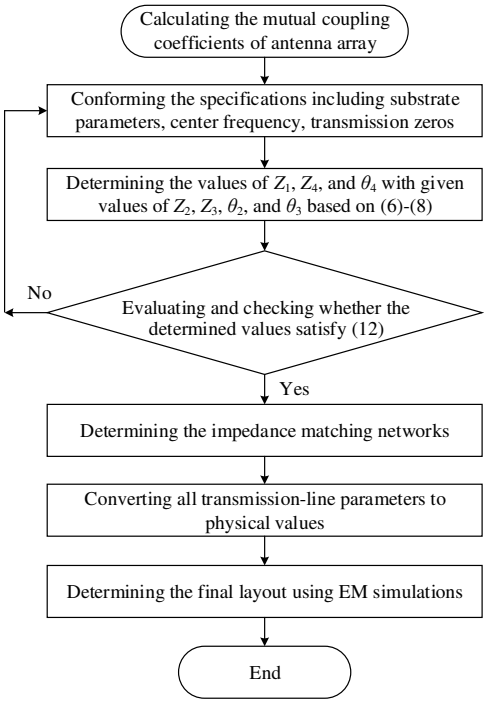

Fig. 7. Design flowchart of the proposed decoupling-filtering network.

Step 4: Determining the impedance matching networks.

Step 5: Determining the physical configuration. Based on the theoretically selected parameter values, the final layout of the decoupling network can be constructed and further optimized through full-wave simulations. In this step, all the situations encountered in practical implementation will be taken into account, involving the influence of the soldering pad of the connectors, the effect of the meandered lines as well as the mutual coupling between transmission lines.

In summary, by using the presented procedure, decoupling networks with filtering responses for linear arrays can be realized. For the 4×4 dual-polarized array shown in Fig. 1, it can be considered as two individual arrays with orthogonal polarizations. Then, a decoupling network can be constructed by extending the proposed scheme. Despite that no decoupling scheme is directly used for the vertically positioned elements, the mutual coupling among these elements is also suppressed to almost less than −25 dB. This is contributed by the filtering responses of the proposed decoupling network, resulting in improved frequency selectivity at the lower- and upper-frequency edges. Consequently, the out-of-band spurious are suppressed, leading to partially suppressed in-band mutual coupling between the vertical pairs. In the next section, numerical studies are going to be operated to further verify this.

III. Further Investigation Using Case Studies

The theoretical investigations described in Section II focus on the decoupling and filtering purposes for horizontally allocated antenna elements, based on numerical derivations. In the section, graphical studies are further carried out to show the visible determination of the two transmission zeros generated

TABLE I
PARAMETER VALUES OF SOME STUDY CASES

Cases	Z_1 (Ω) θ_1 (°)	Z_2 (Ω) θ_2 (°)	Z_3 (Ω) θ_3 (°)	Z_4 (Ω) θ_4 (°)
Case A	50 Ω 73°	81 Ω 446°	86 Ω 136°	83 Ω 78.9°
Case B	50 Ω 64°	78 Ω 429°	99 Ω 136°	84 Ω 78.9°
Case C	50 Ω 66°	66 Ω 409°	98 Ω 150.4°	95 Ω 85.8°
Case D	50 Ω 65°	56 Ω 396°	120 Ω 151.4°	95 Ω 86.4°
Case E	50 Ω 66°	59 Ω 394°	120 Ω 156.6°	95 Ω 87.2°
Case F	50 Ω 64°	61 Ω 394°	97 Ω 142.8°	99 Ω 87°

by the proposed scheme, which will be discussed in Part A. Moreover, the decoupling performance for horizontal, vertical, and diagonal pairs of antenna elements will be shown and discussed in Part B. Some comparison studies between the proposed scheme and a previously published method will also be given.

A. *Transmission zeros*

As discussed in Section II, the filtering response is determined by two given frequency edges f_1 and f_2, as described in (12). Seeing that the proposed decoupling network is integrated with the antenna array in practice, it is not easy to evaluate the transmission performance from the input port of the network to the corresponding antenna element directly. On the other hand, as for the circuit shown in Fig. 4, there should have reflection poles at the two sides of the center frequency, representing the transmission zeros determined by (12). This implies that for the mutual coupling between the decoupled antenna elements, there would also have a transmission zero at each side of the center frequency. At this point, the transmission response between Port 12 and Port 14 of the array in Fig. 1 is selected as the study case to present the filtering responses. The transmission coefficients $S_{14,12}$ with several groups of parameter values are calculated based on (6)-(8) and (12), as listed in Table I. Further, graphical studies are carried out, as sketched in Fig. 8. Notice that all the cases are matched by using the configuration illustrated in Fig. 5, which is not detailed for brevity.

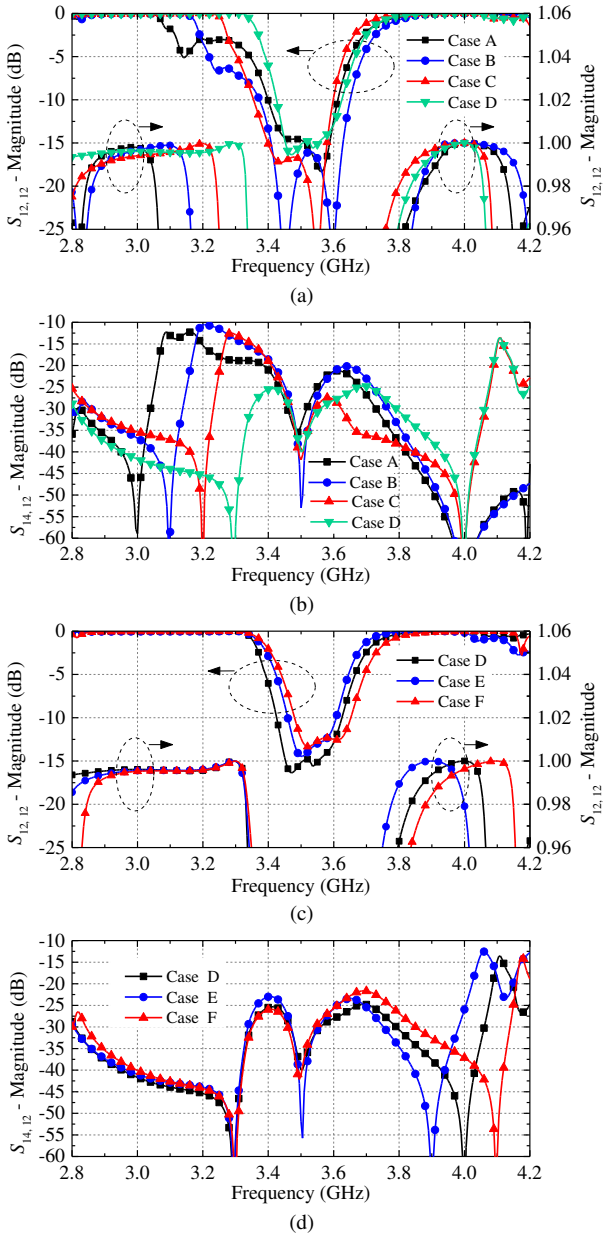

Fig. 8. Graphical studies of the filtering responses of the decoupled 4×4 dual-polarized patch antenna array. (a) and (b) f_2 is locked. (c) and (d) f_1 is locked.

For Cases A, B, C, and D, the upper transmission zero is locked, while the lower one can be tuned by itself. This is similar when the lower transmission zero is specified, as depicted in Fig. 8(d). It is seen that the magnitudes of $S_{12,12}$ of all the study cases are approximately equal to one at the transmission zeros f_1 and f_2. This implies that all the other transmission coefficients among the antenna elements have the same transmission zero positions. The results indicate that the two transmission zeros can be adjusted independently, meanwhile, the decoupling performance at the center frequency 3.5 GHz is not influenced seriously. Note that the decoupling bandwidth is influenced when the transmission zeros are moving. In some cases, the bandwidth can be extended, compared to the original one without decoupling. However, as the transmission zeros get closer to the center frequency, the decoupling level would be better but the impedance bandwidth (constrained between two transmission zeros) becomes narrower. Consequently, there is a tradeoff between the decoupling and impedance bandwidth when determining the transmission zeros f_1 and f_2. The basic consideration is that the passive bandwidth should not be narrowed after decoupling.

Furthermore, parameter sensitivity of the filtering and decoupling performance of the array integrated with the proposed structures is also investigated to give a visible guideline for realization. Here, Case D is selected as the reference study. Fig. 9 illustrates the magnitudes of $S_{14,12}$ varying with the changing of the key parameters based on Case D. Notice that the decoupled antennas are all impedance

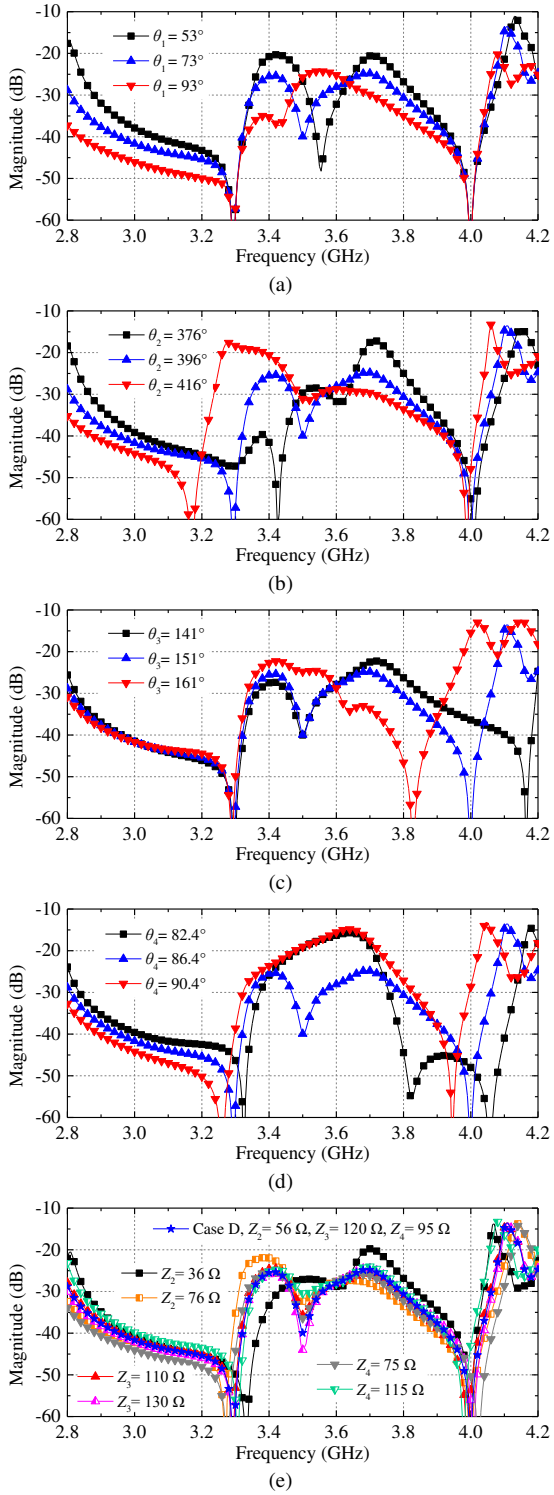

Fig. 9. Parameter sensitivity of the filtering and decoupling performance of the array based on Case D, with the different values of (a) θ_1, (b) θ_2, (c) θ_3, (d) θ_4, and (e) Z_2, Z_3, and Z_4.

matched around the center frequency with $|S_{i,i}| \leq -10$ dB, which are not detailed for brevity. For the decoupling, the operating frequency departs away from the center frequency f_0 when the value of θ_1 changes, but a high decoupling level still holds at the operating frequency as plotted in Fig. 9(a). As for the filtering performance, the transmission zeros at the lower and upper

TABLE II
CALCULATED VALUES OF THE PARAMETERS OF THE PROPOSED SCHEME

Parameters	Values (Ω)	Parameters	Values (°)
Z_1	50	θ_1	70.5
Z_2	73	θ_2	394
Z_3	120	θ_3	150
Z_4	70	θ_4	86.5
Z_{m1}	116	θ_{m1}	114
Z_{m2}	52	θ_{m2}	185.4
Z_{m3}	102	θ_{m3}	84.4
Z_{m4}	85.6	θ_{m4}	157.2

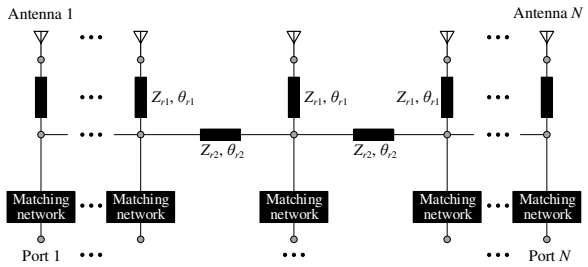

Fig. 10. Decoupling configuration of a referenced scheme based on the method reported in [8], for linear arrays.

frequencies are mainly determined by the electronic lengths of θ_2 and θ_3, respectively. This implies that the rejection band of the decoupled antenna is controlled mainly by θ_2 and θ_3. The influence of changing the values of Z_2, Z_3, and Z_4 on the performance is provided in Fig. 9(e). The transmission responses, including the transmission zeros and the decoupling bandwidth, are tuned slightly, despite that some of the characteristic impedance values change among wide ranges. The aforementioned discussions denote that the rejection and decoupling bands are mainly determined by the electronic lengths of the transmission lines. The characteristic impedance values of the stubs play a fine-tuning role intuitively.

B. Decoupling performance for horizontal, vertical, and diagonal pairs

By following the proposed design procedure, a decoupling network for the dual-polarized antenna array plotted in Fig. 1 is designed. The theoretical values of the parameters are listed in Table II. Then, the decoupling performance between horizontal, vertical, and diagonal pairs of antenna elements can be obtained. Based on the results of Fig. 8 and the discussions in Section II-A, it can be reasonably concluded that the coupling suppression between the vertical or diagonal allocated elements is mainly contributed by the transmission zeros. With the moving of the transmission zeros, the decoupling bandwidth is also changed. Taking Cases A, B, C, and D for example, when the transmission zero at the lower frequency f_1 is moving close to the center frequency f_0, the mutual coupling is suppressed not only at f_1, but also among the band between f_1 and f_2. Therefore, by properly selecting the lower and upper transmission zeros, the coupling between vertical or diagonal elements can also be suppressed more or less. On the other hand, the method presented in [8] can also be utilized to decouple dual-polarized 2-dimension antenna arrays but needs

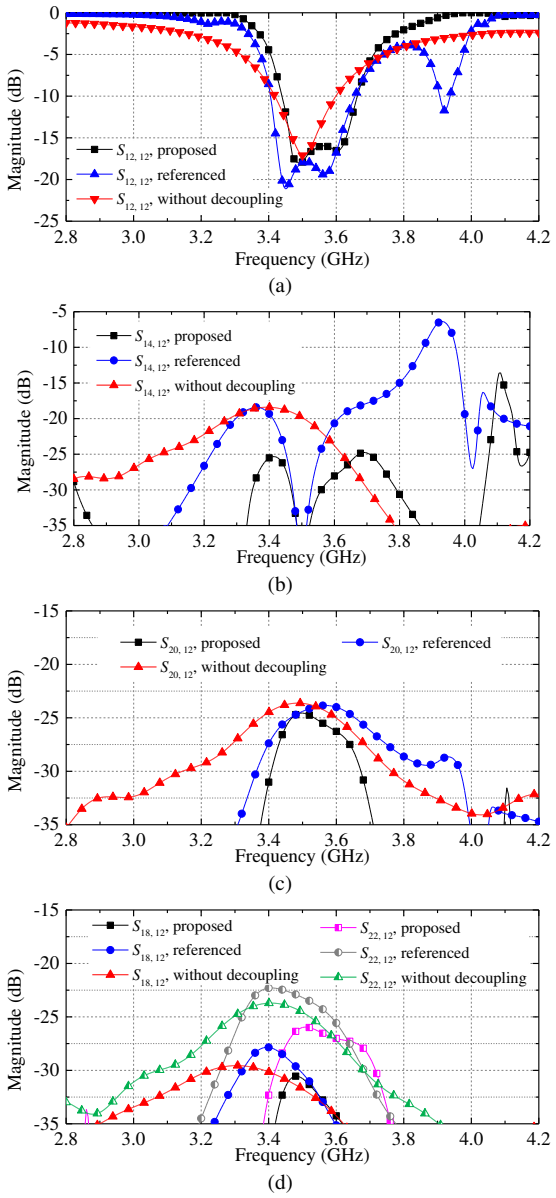

Fig. 11. Calculated mutual coupling of the decoupled 4×4 dual-polarized patch antenna array. (a) $S_{12,12}$. (b) $S_{14,12}$. (c) $S_{20,12}$. (d) $S_{18,12}$ and $S_{22,12}$.

multilayer stackup to place the decoupling network and without any filtering responses. To make an available comparison, the scheme reported in [8] is simplified to decouple the array shown in Fig. 1, as illustrated in Fig. 10 and marked as the referenced scheme. The referenced one is also a 1-dimension method. Replacing the proposed decoupling-filtering scheme shown in Fig. 2 by the referenced one, the 4×4 dual-polarized antenna array can be decoupled for horizontal elements, but without any filtering responses. The same to the proposed scheme, there is no direct decoupling structure for the vertical and horizontal pairs of elements in the referenced scheme.

Fig. 11 illustrates the calculated results of the 4×4 arrays by using the proposed and referenced schemes, based on the equivalent circuits depicted in Fig. 2(b) and Fig. 10 correspondingly. Here, Port 12 is selected as the representative port. Compared to the result without decoupling, the antennas

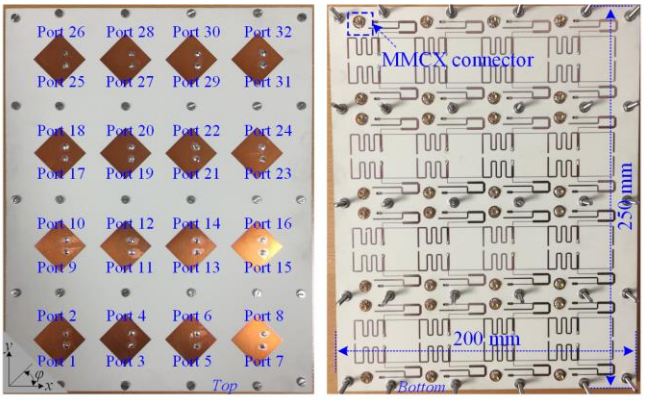

Fig. 12. Photos of the developed array with the proposed decoupling-filtering network.

using the proposed or referenced decoupling methods feature wider impedance bandwidths, as illustrated in Fig. 11(a). The in-band reflection coefficients of the two decoupled arrays are almost less than −15 dB. However, the out-of-band signal is not well-suppressed when using the referenced method, which has been verified in [8]. Thus, the mutual coupling suppression level of the proposed one is much better than the referenced one, when the frequency departs away from 3.5 GHz as revealed from Fig. 11(b). It is observed from Fig. 11(c) and Fig. 11(d) that for the proposed scheme, the mutual coupling among vertical and horizontal pairs are also suppressed or kept at a low level of less than −24.7 dB. In contrast to the proposed scheme, the coupling between the horizontal pair, $S_{20,12}$, is still higher than −24 dB when the referenced scheme is employed, and particularly, the isolation level between diagonal elements is decreased to less than 22.5 dB. Based on the aforementioned discussions, it is numerically verified that the proposed decoupling method is effective for the vertical and diagonal allocated antenna elements, despite that there is no direct decoupling structure for these elements.

In the next section, the design example is fabricated. Full-wave simulated and measured results will be provided to show the practical performance.

IV. Final Design, Measurements and Discussions

After electromagnetic optimization, the physical dimensions are finally determined. The decoupled antenna array is fabricated as shown in Fig. 12. The entire size is 250×200×5.56 mm^3, where the decoupling and filtering network is printed on a single substrate layer with a compact layout. This section includes three parts. In Part A, the measured results of the designed antenna are given and discussed. The array performance under scanning conditions and comparisons with recently published works are provided in Part B and Part C, respectively.

A. Measurements of the array

The proposed array is fully tested by using the Keysight N5227A network analyzer and the in-house SATIMO SG24L spherical near-field scanner. Fig. 13 illustrates the measured impedance matching and mutual coupling responses of the

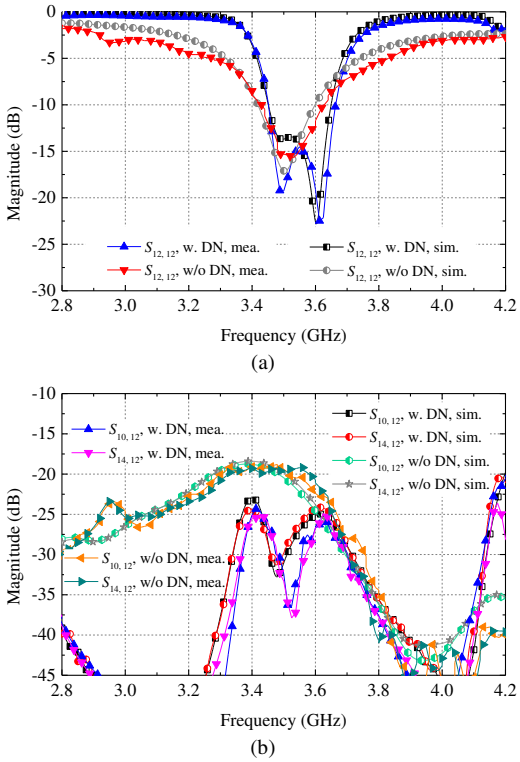

Fig. 13. Measured and simulated (a) impedance matching performance and (b) coupling between adjacent elements along the horizontal direction of the decoupled array.

array, where port 12 is chosen as the representative port. The array without any decoupling or filtering structure is also simulated, measured, and summarized to make a visible performance comparison. It is observed that good frequency selectivity is obtained. The coupling between horizontal pairs is suppressed to less than −25.1 dB, while the maximum level before decoupling is −18.3 dB. Moreover, the out-of-band spurious are also suppressed owing to the introduced filtering responses. As illustrated in Fig. 14(a) and Fig. 14(b), the mutual coupling levels between vertical and diagonal pairs, i.e. $S_{4,12}$ and $S_{22,12}$ correspondingly, are all decreased to less than −25 dB, as expected and numerically verified in Section III. Fig. 14(c) and Fig. 14(d) depict the coupling levels between non-adjacent and cross-polarized elements, respectively. The results denote that for the developed antenna array, all the mutual coupling paths among antenna elements are well-suppressed or kept at a very low level. The spurious are reduced within the studied frequency band, contributed by the additional filtering responses.

The radiation performance is tested, including radiation patterns, maximum realized gain, and total efficiency, which are illustrated in Fig. 15, Fig. 16(a) and Fig. 16(b) correspondingly. To show the out-of-band rejection of the decoupled array, a wide frequency band from 1.5 to 5.5 GHz is selected as the study band. Since there is no additional structure loaded on/around the radiation patches, the radiation patterns of the decoupling array are close to the original one without any decoupling scheme. The measured maximum gain is given in Fig. 16(a), a high frequency selectivity level is achieved, a

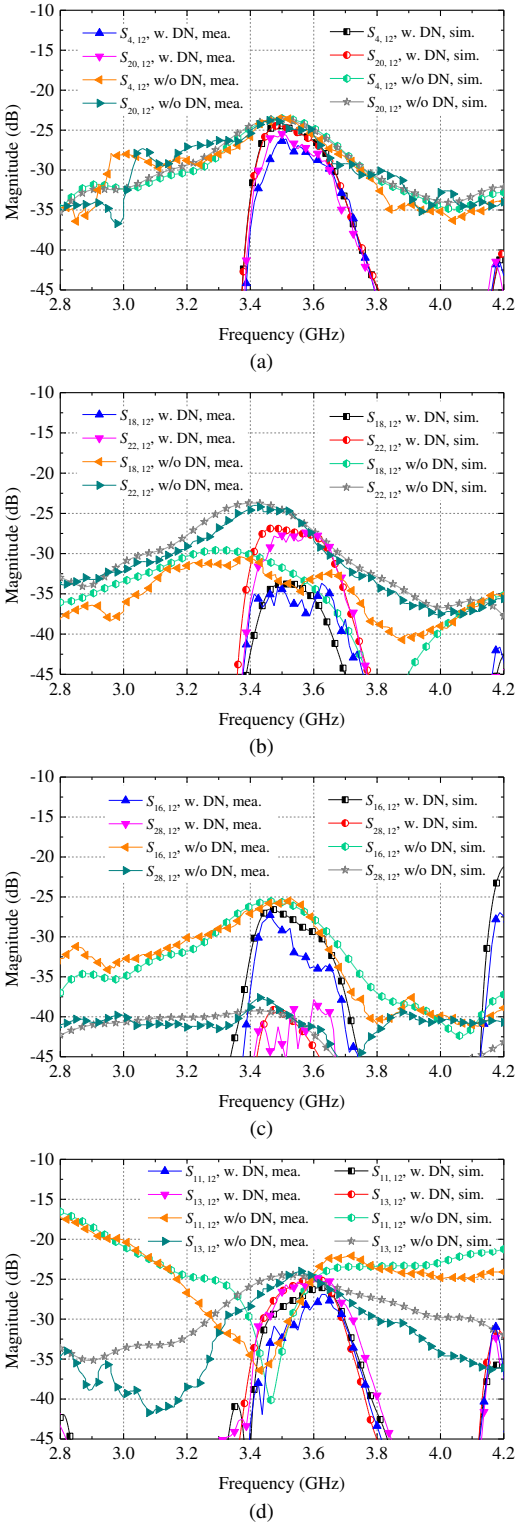

Fig. 14. Measured and simulated mutual coupling among other elements of the decoupled array. (a) $S_{4,12}$ and $S_{20,12}$. (b) $S_{18,12}$ and $S_{22,12}$. (c) $S_{16,12}$ and $S_{28,12}$. (d) $S_{11,12}$ and $S_{13,12}$.

transmission zero is generated at each edge of the passband. Meanwhile, the total efficiency exhibits a bandpass response as well. It is found that the realized gain among the lower spurious frequency band is well-suppressed to almost less than −12.5 dBi. The gain has peaks as the frequency departs from the upper transmission zero points, such as 4.25 GHz and 4.8 GHz.

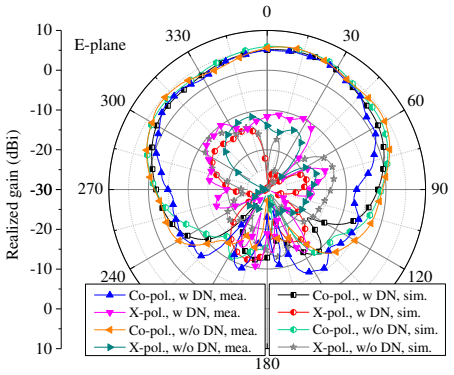

(a)

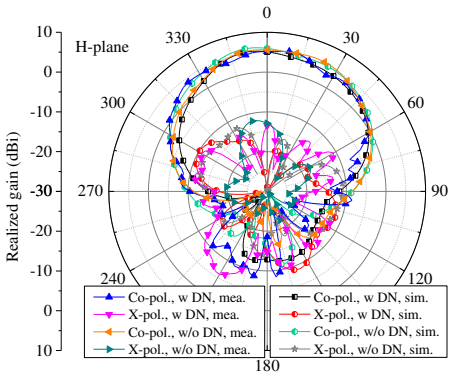

(b)

Fig. 15. Measured and simulated radiation patterns at 3.5 GHz when the representative port is excited. (a) E plane. (b) H plane.

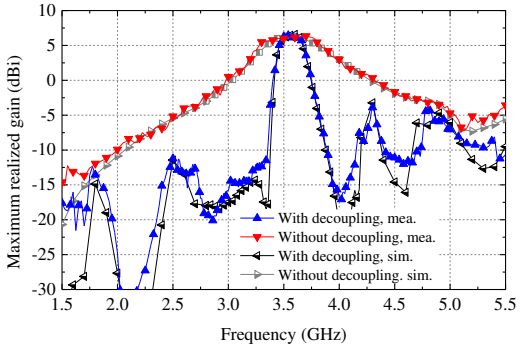

(a)

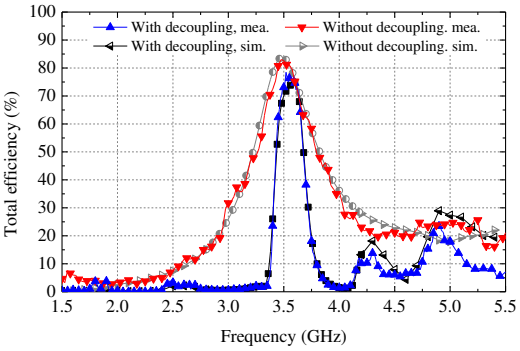

(b)

Fig. 16. Measured and simulated (a) maximum realized gain and (b) total efficiency when the representative port is excited.

Despite this, the maximum gain at the upper stopband is still decreased, compared to the one without decoupling. All the measured results are consistent with the full-wave simulated

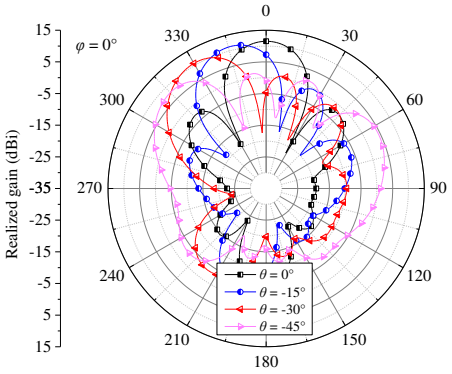

(a)

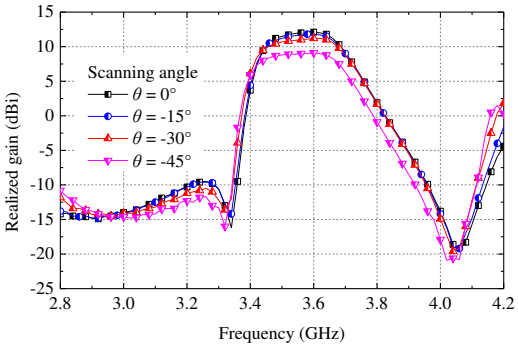

(b)

Fig. 17. (a) Simulated patterns of the proposed array under different beam scanning angles, when ports 10, 12, 14, and 16 are excited. (b) Simulated gains at different beam scanning angles, when ports 10, 12, 14, and 16 are excited.

ones. Around 10% total efficiency loss is observed from Fig. 16(b), which will slightly decrease the MIMO multiplexing efficiency. But with the reduced mutual coupling from around -17 dB to -25 dB, several dBs can be gained from the improved VSWR, high power amplifier efficiency, and integrated filter function. The discussions denote that the developed array features well-designed decoupling and filtering responses, with a low profile and low insertion loss.

Compared to the array without decoupling, a small insertion loss of around 0.6 dB is introduced for the demonstrator, which is mainly introduced by the lossy transmission lines. This would contribute a 1.2-dB improvement to the isolation. For the horizontally-positioned antennas, excluding the transmission losses, the maximum coupling level is less than −23.9 dB after decoupling within the operating frequency band, and the isolation level around the center frequency is still higher than 30 dB, as evaluated from Fig. 13. As for the coupling levels of the decoupled antennas shown in Fig. 14 where the antenna elements are not decoupling directly, they are also suppressed by 1~3 dB even if the transmission losses are excluded. It is believed that the insertion loss of 0.6 dB is acceptable in this article since both decoupling and filtering responses are achieved simultaneously for large-scale antenna arrays. For instance, the decoupling network proposed in [8] introduced a 0.7-dB insertion loss for a 4×4 array without filtering function. It can be concluded that for the decoupled array in [8], simply cascading a filter at the input interface of every decoupled antenna to further achieve filtering function would introduce

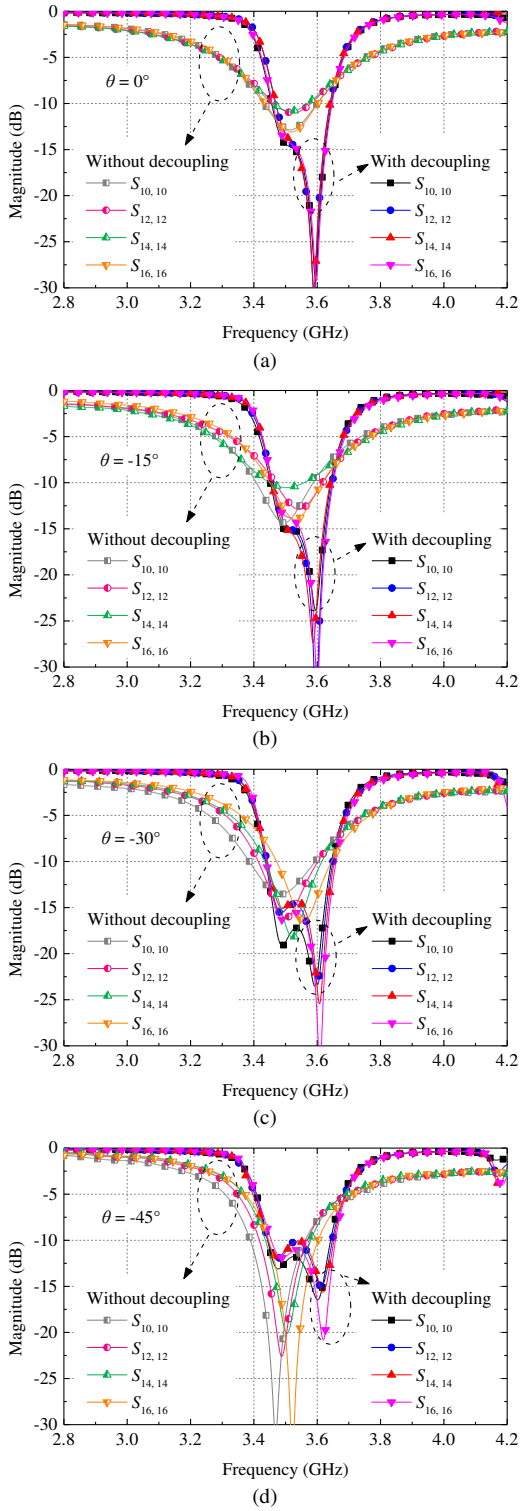

Fig. 18. Simulated active reflection coefficients of the proposed array under different beam scanning angles, when ports 10, 12, 14, and 16 are excited. Beamforming at (a) 0°, (b) −15°, (c) −30°, (d) −45°.

additional insertion losses by the filter.

B. *Scanning performance*

In this part, the beam scanning performance of the decoupled array is further investigated. For ease of study, ports 10, 12, 14, and 16 are selected as the representative ports. Fig. 17(a) describes the radiation patterns scanned from 0° to 45°, at 3.5 GHz. A 2.7-dB gain reduction from θ = 0° to θ = −45° is observed, mainly due to the gain degradation of the radiation pattern of the antenna elements. The realized gains against frequencies at different scanning angles are given in Fig. 17(b). Despite small insertion losses, good selectivity is still kept as expected.

The active reflection coefficients of the arrays with and without the decoupling networks are also simulated, as illustrated in Fig. 18. The active impedance matching of the array without decoupling is unstable under scanning conditions. For instance, port 14 is almost mismatched with the scanning angle of 15°. The common active impedance bandwidth before decoupling is dramatically decreased. Moreover, the result implies that the effect of the mutual coupling on the active impedance matching of the antenna elements is random. Compared to the array without decoupling, the decoupled one features more stable responses. The common active impedance bandwidth is not narrowed and almost the same as the passive result recorded in Section IV-A. Particularly, there is nearly no offset between different reflection curves apparently from these results. In a word, after integrating the proposed decoupling networks, the array is well-matched with stable frequency selectivity.

TABLE III
COMPARISONS BETWEEN THE PROPOSED DECOUPLING SCHEME AND SOME RECENTLY PUBLISHED WORKS

Ref.	Decoupling Method	Array Configuration	Antenna Polarization	Filtering Response
[7]	Network	1-D	single	No
[8]	Network	2-D	Dual	No
[9]	Surface	2-D	Dual	No
[19]	Network	1-D	Single	No
[21]	Weak field	1-D	Single	No
[22]	Resonator	1-D	Single	No
[23]	Wavetrap	2-D	Single	No
This work	Network	2-D	Dual	Yes

C. *Summarized Comparisons*

Here, some recently published decoupling methods for large-scale antenna arrays are summarized for comparison purposes, as listed in Table III. The schemes presented in [7], [19], [21], and [22] are employed for 1-dimension array configurations. This means that they are useful for linear antenna arrays, but may not effective for M×N (2-Dimension) arrays. Besides, the methods reported in [8] and [9] can be employed for decoupling dual-polarized arrays, and the rest of the methods focus on single-polarized configurations. Moreover, there is no filtering response in all of the published works listed here. As for the proposed decoupling method, it is available for dual-polarized 2-dimension antenna arrays, and additional bandpass responses are generated from the realized gain point of view, exhibiting well-designed filtering functions. Besides, the proposed method can also be applied in the case of

smaller inter-element distance or other types of antenna elements since the design procedure is independent of antenna types and array configurations.

V. Conclusion

A simple and compact decoupling method with a filtering response is proposed for patch antenna arrays in this work. Specifically, the proposed scheme is not a combination of decoupling and filtering networks, but is achieved by a T-shaped transmission-line-based architecture that contributes both the filtering and decoupling responses. Theoretical analysis and full-wave simulations are operated to verify the performance of the proposed network, along with a design procedure for implementation purposes. A demonstrator is further manufactured and measured to display the practical decoupling and filtering levels. Besides, scanning responses of the decoupling array are also investigated, which shows a well-matched impedance matching and very stable frequency selectivity. Moreover, there is no additional structure loaded on or around the radiating structures, leading to a low profile and a very small influence on the radiation patterns. Both the simulated and measured results show that the presented scheme features compact physical sizes and low insertion losses, making it available for large-scale arrays to realize the desired responses.

References

[1] B. Wang, Y. Chang, and Y. Sun, "Performance of the large-scale adaptive array antennas in the presence of mutual coupling," *IEEE Trans. Antennas Propag.*, vol. 64, no. 6, pp. 2236-2245, Jun. 2016.

[2] R. Janaswamy, "Effect of element mutual coupling on the capacity of fixed length linear arrays," *IEEE Antennas Wireless Propag. Lett.,* vol. 1, pp. 157-160, 2002.

[3] D. M. Pozar, "Relation between the active input impedance and the active element pattern of a phased array," *IEEE Trans. Antennas Propag.*, vol. 51, no. 9, pp. 2486-2489, Sep. 2003.

[4] C. Fager, X. Bland, K. Hausmair, et al. "Prediction of smart antenna transmitter characteristics using a new behavioral modeling approach," *IEEE MTT-S Int. Microw. Symp.*, Tampa, FL, Jun. 1-6, 2014, pp. 1-4.

[5] X. Chen, S. Zhang, and Q. Li, "A review of mutual coupling in MIMO systems." *IEEE Access*, vol. 6, pp. 24706-24719, 2018.

[6] L. Savy and M. Lesturgie, "Coupling effects in MIMO phased array," in *Proc. IEEE Radar Conf.* (*RadarConf*), Philadelphia, PA, USA, May 2016, pp. 1–6.

[7] R.-L. Xia, S.-W. Qu, P.-Fa Li, D.-Q. Yang, S. Yang, and Z.-P. Nie, "Wide-angle scanning phased array using an efficient decoupling network," *IEEE Trans. Antennas Propag.*, vol. 63, no. 11, pp. 5161-5165, Nov. 2015.

[8] Y.-M. Zhang, S. Zhang, J.-L. Li, and G. F. Pedersen, "A transmission-line-based decoupling method for MIMO antenna arrays," *IEEE Trans. Antennas Propag.*, vol. 67, no. 5, pp. 3117-3131, May 2019.

[9] K.-L. Wu, C. Wei, X. Mei, and Z.-Y. Zhang, "Array-antenna decoupling surface," *IEEE Trans. Antennas Propag.*, vol. 65, no. 12, pp. 6728-6738, Dec. 2017.

[10] X. Tan, W. Wang, Y. Wu, Y. Liu, and A. A. Kishk, "Enhancing isolation in dual-band meander-line multiple antenna by employing split EBG structure," *IEEE Trans. Antennas Propag.*, vol. 67, no. 4, pp. 2769-2774, Apr. 2019.

[11] H. Meng and K.-L. Wu, "An LC decoupling network for two antennas working at low frequencies," *IEEE Trans. Microw. Theory Techn.*, vol. 65, no. 7, pp. 2321–2329, Jul. 2017.

[12] J. Sui and K.-L. Wu, T. Li and X. Gong, "A general T-stub circuit for decoupling of two dual-band antennas," *IEEE Trans. Microw. Theory Tech.*, vol. 65, no. 6, pp. 2111-2121, Jun. 2017.

[13] Y.-F. Cheng and K.-K. M. Cheng, "A novel dual-band decoupling and matching technique for asymmetric antenna arrays," *IEEE Trans. Microw. Theory Tech.*, vol. 6, no. 5, pp. 2080-2089, May. 2018.

[14] M. Li, L. Jiang, and K. L. Yeung, "Novel and efficient parasitic decoupling network for closely coupled antennas," *IEEE Trans. Antennas Propag.*, vol. 67, no. 6, pp. 3574-3585, Jun. 2019.

[15] F. Liu, J. Guo, L. Zhao, G.-L. Huang, Y. Li, and Y. Yin, "Dual-band metasurface-based decoupling method for two closely packed dual-band antennas," *IEEE Trans. Antennas Propag.*, vol. 68, no. 1, pp. 552-557, Jan. 2020.

[16] D. Gao, Z.-X. Gao, S.-D. Fu, X. Quan, and P. Chen, "A novel slot-array defected ground structure for decoupling microstrip antenna array," *IEEE Trans. Antennas Propag.*, 2020. DOI: 10.1109/TAP.2020.2992881

[17] X. Yu, and H. Xin, "Direction-of-arrival estimation enhancement for closely spaced electrically small antenna array," *IEEE Trans. Microw. Theory Tech.*, vol. 66, no. 1, pp. 477-484, Jan. 2018.

[18] J. Weber, C. Volmer, K. Blau, R. Stephan, and M. A. Hein, "Miniaturized antenna arrays using decoupling networks with realistic elements," *IEEE Trans. Microw. Theory Tech.*, vol. 54, no. 6, pp. 2733-2740, Jun. 2006.

[19] X.-J. Zou, G.-M. Wang, Y.-W. Wang, and H.-P. Li, "An efficient decoupling network between feeding points for multielement linear arrays," *IEEE Trans. Antennas Propag.*, vol. 67, no. 5, pp. 3101-3108, May 2019.

[20] C. Wei, Z.-Y. Zhang, and K.-L. Wu, "Phase compensation for decoupling of large-scale staggered dual-polarized dipole array antennas," *IEEE Trans. Antennas Propag.*, vol. 68, no. 4, pp. 2822-2831, Apr. 2020.

[21] H. Lin, Q. Chen, Y. Ji, X. Yang, J. Wang, and L. Ge, "Weak-field-based self-decoupling patch antennas," *IEEE Trans. Antennas Propag.*, vol. 68, no. 6, pp. 4208-4217, Jun. 2020.

[22] M. Li, B. G. Zhong, and S. W. Cheung, "Isolation enhancement for MIMO patch antennas using near-filed resonators as coupling-mode transducers," *IEEE Trans. Antennas Propag.*, vol. 67, no. 2, pp. 755-764, Feb. 2019.

[23] Y.-M. Zhang, S. Zhang, J.-L. Li, and G. F. Pedersen, "A Wavetrap-Based Decoupling Technique for 45°-Polarized MIMO Antenna Arrays," *IEEE Trans. Antennas Propag.*, vol. 68, no. 3, pp. 2148-2157, Mar. 2020.

[24] Y.-T. Liu, K. W. Leung, and N. Yang, "Compact absorptive filtering patch antenna," *IEEE Trans. Antennas Propag.*, vol. 68, no. 2, pp. 633-642, Feb. 2020.

[25] P. F. Hu, Y. M. Pan, X. Y. Zhang, ang B. J. Hu, "A compact quasi-isotropic dielectric resonator antenna with filtering response," *IEEE Trans. Antennas Propag.*, vol. 67, no. 2, pp. 1294-1299, Feb. 2019.

[26] W. Yang, S. Chen, Q. Xue, W. Che. G. Shen, and W. Feng, "Novel filtering method based on metasurface antenna and its application for wideband high-gain filtering antenna with low profile," *IEEE Trans. Antennas Propag.*, vol. 67, no. 3, pp. 1535-1544, Mar. 2019.

[27] C.-K. Lin, and S.-J. Chung, "A filtering microstrip antenna array," *IEEE Trans. Microw. Theory Tech.*, vol. 59, no. 11, pp. 2856-2863, Nov. 2011.

[28] R. E. Lovato, T. Li and X. Gong, "Tunable filter/antenna integration with bandwidth control," *IEEE Trans. Microw. Theory Tech.*, vol. 67, no. 10, pp. 4196-4205, Oct. 2019

[29] Y.-M. Zhang, S. Zhang, G. Yang and G. F. Pedersen, "A wideband filtering antenna array with harmonic suppression," *IEEE Trans. Microw. Theory Tech.*, vol. 68, no. 10, pp. 4327-4339, Oct. 2020

[30] H.-T. Hu, F.-C. Chen, J.-F. Qian, and Q.-X. Chu, "A differential filtering microstrip antenna array with intrinsic common-mode rejection," *IEEE Trans. Antennas Propag.*, vol. 65, no. 12, pp. 7361-7365, Dec. 2017.

[31] D. M. Pozar, "Microwave network analysis," in *Microwave Engineering*, 4th ed. Hoboken, NJ, USA: Wiley, 2012, ch. 4, pp. 188-194.

[32] D. A. Frickey, "Conversions between S, Z, Y, H, ABCD, and T parameters which are valid for complex source and load impedances," *IEEE Trans. Microw. Theory Tech.*, vol. 42, no. 2, pp. 205-211, Feb. 1994.